

# The Discovery of GIT1/ $\beta$ -Pix Inhibitors: Virtual Screening and Biological Evaluation of New Small-molecule Compounds with Anti-invasion Effect in Gastrointestinal Neoplasms

Chenkun Wang<sup>1,2,\*</sup>, Jing Gu<sup>2,\*</sup>, Hongwei Li<sup>2,\*</sup>, Bo Zhao<sup>2</sup>, Tao Yu<sup>1,2</sup>, Chun-Ling Guo<sup>2</sup>, Mouxin Huang<sup>2</sup>, Weiwei Jiang<sup>1</sup>, Qin Ouyang<sup>2</sup>

<sup>1</sup>Department of Pharmacy, the Second Affiliated Hospital, Chongqing Medical University, Chongqing, People's Republic of China; <sup>2</sup>Department of Medicinal Chemistry, College of Pharmacy, Third Military Medical University, Chongqing, People's Republic of China

\*These authors contributed equally to this work

Correspondence: Weiwei Jiang, Department of Pharmacy, the Second Affiliated Hospital, Chongqing Medical University, No. 1 Yixueyuan Road, Yuzhong District, Chongqing, 400010, People's Republic of China, Email 304035@cqmu.edu.cn; Qin Ouyang, Department of Medicinal Chemistry, College of Pharmacy, Third Military Medical University, No. 30 Gaotanyan St., Shapingba District, Chongqing, 400038, People's Republic of China, Email ouyangq@tmmu.edu.cn

**Background and Objective:** GIT1 (G-protein-coupled receptor kinase interacting protein-1) has been found to be highly related with cancer cell invasion and metastasis in many cancer types.  $\beta$ -Pix (p21-activated kinase-interacting exchange factor) is one of the proteins that interact with GIT1. Targeting GIT1/ $\beta$ -Pix complex might be a potential therapeutic strategy for interfering cancer metastasis. However, at present, no well-recognized small-molecule inhibitor targeting GIT1/ $\beta$ -Pix is available. Thus, we aim to discover novel GIT1/ $\beta$ -Pix inhibitors with simple scaffold, high activity and low toxicity to develop new therapeutic strategies to restrain cancer metastasis.

**Methods:** GIT1/ $\beta$ -Pix inhibitors were identified from *ChemBridge* by virtual screening. Briefly, the modeling of GIT1 was performed and the establishment of GIT1/ $\beta$ -Pix binding pocket enabled the virtual screening to identify the inhibitor. In addition, direct binding of the candidate molecules to GIT1 was detected by biolayer interferometry (BLI) to discover the hit compound. Furthermore, the inhibitory effect on invasion of stomach and colon cancer cells in vitro was carried out by the transwell assay and detection of epithelial-mesenchymal transition (EMT)-related proteins. Finally, the binding mode of hit compound to GIT1 was estimated by molecular dynamics simulation to analyze the key amino residues to guide further optimization.

**Results:** We selected the top 50 compounds from the *ChemBridge* library by virtual screening. Then, by skeleton similarity analysis nine compounds were selected for further study. Furthermore, the direct interaction of nine compounds to GIT1 was detected by BLI to obtain the best affinitive compound. Finally, 17302836 was successfully identified ( $K_D = 84.1 \pm 2.0 \mu\text{M}$ ). In vitro tests on 17302836 showed significant anti-invasion effect on gastric cancer and colorectal cancer.

**Conclusion:** We discovered a new GIT1/ $\beta$ -Pix inhibitor (17302836) against gastrointestinal cancer invasion and metastasis. This study provides a promising candidate for developing new GIT1/ $\beta$ -Pix inhibitors for tumor treatment.

**Keywords:** hit discovery, virtual screening, GIT1,  $\beta$ -Pix, gastrointestinal cancers, invasion

## Introduction

Gastrointestinal cancers including gastric cancer and colorectal cancer are the third and fifth leading cause of cancer deaths in China, respectively.<sup>1</sup> Metastasis is the main cause of their progression and mortality.<sup>2</sup> To discover new targets and therapeutic agents for intervening metastasis has been long focused and deemed as promising strategies for cancer treatment. Small G proteins, such as the ADP-ribosylation factor (Arf) family proteins and Rho family proteins, play an

important role in cell migration by controlling cytoskeleton aggregation and deaggregation.<sup>3,4</sup> Small G proteins could be activated or deactivated via binding or hydrolysis of GTP, which are mediated by guanine nucleotide exchange factor (GEF) and GTPase-activating protein (GAP), respectively. Therefore, GAP and GEF are key regulatory factors that influence cell adhesion, cell polarity and cell migration.<sup>5,6</sup>

GIT, a scaffold protein including GIT1 and GIT2, is the GAP protein for Arf small GTP-binding proteins, can limit the activity of Arf proteins.<sup>7</sup> In contrast,  $\beta$ -Pix is the GEF protein for the Rho family small G protein members Rac1 and Cdc42, function to enhance the activity of Rho small G proteins.<sup>7</sup> GIT1 regulates many physiological and pathological processes including enhancing angiogenesis to promote fracture healing,<sup>8</sup> spinal cord ischemia-reperfusion injury,<sup>9,10</sup> schizophrenia,<sup>11,12</sup> etc, through multiple signal pathways. Previous studies suggested that GIT1 overexpression was correlated with stronger ability of invasion and metastasis in multiple types of malignant neoplasms, including liver, lung, gastric cancers, melanoma, and osteosarcoma.<sup>13–17</sup> While knockdown of GIT1 in these cancer cells significantly retarded their invasion and metastasis.<sup>13–17</sup> Moreover, the interaction of  $\beta$ -Pix with GIT1 was vital in the progression of tumor invasion and metastasis.<sup>15,18</sup> GIT and PIX proteins can also form complexes that are recruited to focal adhesion by paxillin, thus regulate cytoskeleton assembly and depolymerization through synergistic regulation of Arf GTPase and Rho GTPase pathways, thereby regulating cell adhesion, cell polarity and cell migration. It is closely related to the occurrence and progression of cancers, especially the invasion and metastasis.<sup>6,7,19</sup> Inhibiting the interaction between GIT1 and  $\beta$ -Pix are proved to effectively interfere the invasion of human gastric cancer<sup>15</sup> and lung adenocarcinoma cells.<sup>18</sup>

Thus, GIT1/ $\beta$ -Pix is a promising therapeutic target to inhibit tumor invasion and metastasis. However, small-molecule inhibitors targeting GIT1/ $\beta$ -Pix are rare, due to the flat interface of protein-protein interaction is challenging for drug discovery. Recently, our group developed the first small-molecule GIT1/ $\beta$ -Pix inhibitor and proved its activity in inhibiting the metastasis of gastric cancer. But its effective concentration is still high for drug use and its scaffold is too complex for further development as drug.<sup>15</sup> Therefore, the discovery of more GIT1/ $\beta$ -Pix inhibitors with simpler scaffold, higher activity and lower toxicity is of great significance for developing new drugs for targeting GIT1/ $\beta$ -Pix to provide new therapeutic strategies to interfere cancer metastasis.

The discovery of lead compounds is the basis for the development of small-molecule antitumor drugs, which are mainly obtained from two approaches: target-based drug discovery (TDD) and phenotypic drug discovery (PDD). In the present study, based on a TDD strategy, we successfully identified a small-molecule inhibitor targeting GIT1/ $\beta$ -Pix protein complex by virtual screening<sup>20</sup> plus direct binding detection. The new candidate molecule 17302836 binds to GIT1 with a moderate affinity, but its relatively high activity against gastrointestinal cancer invasion and metastasis was verified in vitro.

## Materials and Methods

### Modeling of the GIT1 Protein

The X-ray structure of mouse GIT2 (aa.6–358) was downloaded from the Research Collaboratory for Structural Bioinformatics (RCSB) protein database (<https://www.rcsb.org/>, PDB ID: 6JMT). The protein sequence of human GIT1 was obtained from the UniPort protein database (<https://www.uniprot.org/Q9Y2X7>). Robetta, AlphaFold, Swiss-Model and I-TASSER webserver were applied to construct the three-dimensional (3D) structure model. The top-scored structure of each server was evaluated by the UCLA-DOE LAB-SAVES v 6.0 server with ERRAT, VERIFY 3D and PROCHECK methods. The highest-scored model of each method was selected for quality assessment. The visualization of the predicted structure models was performed using the PyMOL program (Schrodinger, LLC, 2015).

### Molecular Docking

For GIT1/ $\beta$ -Pix, the coordinates of the crystallographic structure of the GIT2/ $\beta$ -Pix (PDB code: 6JMT) were used as docking template. Then, the modelled GIT1 structure was superposed to the coordinates of the GIT2 by PyMOL to obtain the GIT1/ $\beta$ -Pix complex. The energy minimizations of the generated structure were employed using Sybyl-X 2.0 with the Powell method under AMBER7 FF99 force field and AMBER charges. The energy minimizations were

terminated when the iterations reached 10,000 steps or the energy gradient less than 0.5 kcal/mol. The processed complex was further optimized by molecular dynamic simulation.<sup>21</sup>

For docking of GIT1 and 17302836, the compound was prepared by Chem 3D 20.0 and GaussView 6.0.16 to optimize the configuration and minimize the energy. Then protein-molecule docking was performed between the prepared GIT1 protein and the optimized compound using software Sybyl-X 2.0 to gain the docked complex.<sup>22</sup>

## Virtual Screening

Virtual screening (VS) is a drug discovery strategy that searches libraries of small molecules for structures with the highest probability of binding to a drug target.<sup>23</sup> Based on the established binding pocket of GIT1, a virtual screening was initiated to identify GIT1/ $\beta$ -Pix inhibitors with novel structure and potential activity from the *ChemBridge* database with 1.3 million compounds. In brief, the protein GIT1 was prepared by Sybyl-X 2.0 software. The binding pocket was generated by scanning the mutichannel surface and LEU271 and LEU279 were selected to generate the binding pocket. The screening was performed using Sybyl-X 2.0 software with Surflex-Dock (SFXC) mode. Compounds with docking scores cut-off at 8.0 were chosen for a further docking using Surflex-Dock Geomx (SFXC) mode in Sybyl-X 2.0. Eventually, nine candidates were purchased among 50 top ranked compounds the for follow-up studies.

## Compound Sources

Compounds for screening test were purchased from Topscience (Shanghai, China). A larger quantity of 17302836 was synthesized following literature procedures and identified by <sup>1</sup>H-NMR and <sup>13</sup>C-NMR. All final compounds were determined by HPLC analysis to achieve a purity of > 95%.

## Molecular Dynamics Simulation

Molecular dynamics (MD) simulations were conducted for the docked complex using AMBER20 with ff19SB force field for protein and gaff force field for small molecule.<sup>24,25</sup> TLEaP module and pmemd.MPI were used to prepare the structures and minimize the structures, respectively. After minimization and equilibration, MD simulations for the different systems were implemented, respectively. The system was performed under periodic boundary conditions using NPT ensemble at 300 K, 0.9% NaCl and pH 7.5. Then the system was solvated in the OPC water model and subsequently placed into a regular hexahedron box with a minimal distance of 8 Å for the solute from the box borders.

## Trajectory Analysis

The simulation trajectories were analyzed by using the CPPTRAJ module of AMBER 2020. The root mean square deviation (RMSD) and root mean square fluctuation (RMSF) were calculated to evaluate the equilibrium of the system. After the protein reached equilibrium, the average structures of the models were generated by using the CPPTRAJ module. The binding interactions between GIT1 and compound 17302836 were characterized using LigPlot+.<sup>26,27</sup>

## Calculation of Binding Free Energies

To calculate the binding free energies of GIT1 and compound 17302836, 100 ns MD simulation was performed using the MD protocol until the system reached equilibrium. The binding free energies were calculated using the MM/GBSA<sup>28</sup> method implemented in AMBER 2020. One hundred snapshots were extracted from the equilibrium trajectory for MM/GBSA free energy calculation. Per-residue energy decomposition was also performed to evaluate the energy contribution of each residue.

## Bi-layer Interferometry (BLI)

The direct interaction between GIT1 and small-molecule compounds was measured by ForteBio Octet RED (Sartorius, Germany). GIT1 (1.0 mg/mL) was biotin-labeled using an EZ-Link™ NHS-PEG4-Biotin kit (#A39259, ThermoFisher, USA) following the manufacturer's protocols. GIT1 concentration was adjusted with PBST (0.05% Tween 20) to 100 µg/mL, then the biotinized protein was fixed to Octet SA biosensors (Sartorius, Germany) in PBST (0.05% Tween 20) buffer

until the binding signal was at least 4 nm, after which the biosensors were rehydrated for 10 min, and the biosensors were transferred to PBST buffer until the baseline was stable.

Each small-molecule compound was diluted with PBST (0.05% Tween 20, containing 0.1% bovine serum albumin and 1.0% DMSO) to 400, 200, 100, 50, and 25  $\mu\text{M}$ , respectively, a solvent control (0  $\mu\text{M}$ ) was also prepared. Then the binding between GIT1 and compounds were on the Octet BLI Discovery platform. This process included an equilibrium (600 s), baseline (60 s), association (200 s), and dissociation (200 s) step in sequence. BLI responses during the whole process were recorded. In addition, to avoid the nonspecific binding, blank SA sensors (no protein fixed) were set as reference for subtraction.

Statistical analysis was performed using Octet Analysis Studio software (Sartorius, Germany) with double-reference subtraction method and 1:1 model to calculate combination-related parameters such as the  $K_D$  value.

## Cell Culture

Human colorectal cancer cell line HCT116 and human gastric cancer cell line MGC803 were provided by the Department of Gastroenterology, Xinqiao Hospital, Third Military Medical University (Chongqing, China), and authenticated by STR profile. The use of the cell line was approved by the Ethics Committee of Third Military Medical University. Cells were cultured in DMEM (ThermoFisher) medium containing 10% fetal bovine serum (Lonsera, URY), 1% penicillin/streptomycin (ThermoFisher). And cells were incubated at 37 °C under a 5% CO<sub>2</sub> atmosphere and passaged when the cell confluence reached 80%.

## Detection of the Cytotoxicity of 17302836

The cytotoxicity of 17302836 against HCT15 and HCT116 cell lines were detected by cell counting kit-8 (CCK-8) assay. Cells were seeded into 96-well plates at a density of 5,000 cells/well and cultured overnight. After the cell attached, 17302836 was added at concentrations of 4.0, 8.0, 16, 24, 32, 50, 60, 80, 100  $\mu\text{M}$  and cells were incubated for 24 h. Then each well was added with 10% CCK-8 reagent (APExBIO, USA) and incubated at 37 °C for 1.5 h in the incubator. The absorbance was measured on a Multi-Mode Detection Platform (SpectraMax Paradigm, Molecular Devices, USA) at 450 nm to calculate the cell viability or cell inhibition rate.

## Western Blotting Assay of Cell Lysate Extracts

Cells were lysed using RIPA lysate (Beyotime, China) with protease inhibitors and phosphatase inhibitors (Beyotime, China) and collected using cell scalper. The total cell extracts were cleaved at 4 °C for 30 min, then centrifuged at 17,000g for 10 min, and the precipitated pellets were removed. The total proteins in the lysate supernatant were quantified by BCA kit (Beyotime, China) to regulate the protein concentration of the samples. Four times loading buffer (Bio-Rad, USA) with the addition of 10%  $\beta$ -mercaptoethanol was added and the protein was denatured at 95 °C for 10 min. Prepared samples containing 30  $\mu\text{g}$  protein were subjected to 8% or 10% SDS-PAGE (Bio-Rad, USA), and proteins were transferred onto 0.22  $\mu\text{m}$  PVDF membrane (Bio-Rad, USA). The membranes were incubated overnight at 4 °C with the corresponding primary antibody including  $\beta$ -tubulin (Cell Signaling Technology, CST#2128S, 1:1000 dilution), ZO-1 (CST#8193T, 1:1000 dilution), N-cadherin (CST#13116S, 1:1000 dilution) and E-cadherin (CST#3195S, 1:1000 dilution), followed by rabbit secondary antibody (Bio-Rad#1,706,515, 1:3000 dilution) at room temperature for 1.5 h. Finally, proteins were visualized using chemiluminescence kit (Beyotime, China) in the chemiluminescence imaging system (Vilber, France), and analyzed quantitatively using the system's analysis software EvolutionCapt-v18.12.

## Transwell Assay

Transwell assay was performed in 24-well plate (Corning, USA) using an 8  $\mu\text{m}$  porechamber (Corning, USA) coated with diluted Matrigel (Corning, USA) (for HCT116, 1:10 diluting ratio was applied, and for MGC803, 1:4 was applied). Cells were starved and treated with the compound in indicated concentrations in serum-free DMEM medium with 0.3% DMSO (Thermo Fisher Scientific, USA) overnight, then 200  $\mu\text{L}$  containing  $1.0 \times 10^5$  (for HCT116) or  $3.0 \times 10^4$  (for MGC803) were seeded onto the upper chamber. The lower chambers were filled with 10% serum-DMEM medium. After incubating at 37 °C for 24 h, the cells that had invaded to the lower surface of the filter were fixed with 4% paraformaldehyde and

stained with 0.1% crystal violet and rinsed with PBS buffer. Finally, cells on the upper surface of the filter were wiped off with a cotton swab, and the cells on the lower surface were recorded and counted under microscope.

## Statistical Analysis

The statistical analysis was performed using GraphPad Prism 8.0 software. Data of cell-based assays were presented as mean  $\pm$  SD stemming from  $\geq 5$  biologically independent experiments, number of replicates were indicated in each figure caption. In addition, two-tailed *t*-tests and one-way ANOVA were conducted to compare the difference between two or multiple groups, respectively. The *P*-value  $< 0.05$  was considered statistically significant.

## Results

### The Molecular Modeling of GIT1/ $\beta$ -Pix

Previous study has demonstrated that GIT1 of the *Homo sapiens* is a multidomain scaffold protein for regulating cell shape and migration. The domains include a N-terminal zinc-finger ArfGAP domain (aa.1–124), an ankyrin repeats (ANK1-3, aa.132–228), a Spa2 homology domain (SHD) domain (aa.264–358), a coiled-coil domain (denoted as the CC Domain, aa.409–473) and a C-terminal focal adhesion targeting (FAT) domain (aa.643–755). In addition to the above domains, the protein also has some disordered regions (aa.354–416, 471–501, 572–606). As the crystal structure of human GIT1 has not been solved yet, the modeling of GIT1 was first performed.

Since the binding between GIT and  $\beta$ -Pix is mainly mediated by the SHD domain, the region of amino acid 8–354 was selected for protein model construction.<sup>19</sup> To generate a reasonable protein model, a total of four protein models were built by Robetta, AlphaFold, Swiss-Model, I-TASSER, respectively. Since the structure of mouse GIT2 was reported in 2020,<sup>19</sup> we performed the amino acid sequences alignment between human GIT1 and mouse GIT2 (PDB ID: 6JMT) using the Clustal W algorithm (Figure 1A).<sup>29,30</sup> It is shown that the sequence in identity is 84.9% (298/351) and 93.2% (327/351) for similarity. Therefore, the 3D structures of GIT1 models were aligned to the crystal structure of GIT2 from *Mus musculus* to compare the differences of protein structures. It is shown that the helix of the models was consistent to the GIT2 crystal structure and aligned well except for the flexible loop region. Referring to the zinc ion of GIT2 protein, the zinc ion of GIT1 protein model is also modelled to the corresponding GIT1 protein position (Figure 1B).

To determine the protein models for further docking and molecular dynamic simulation study, the generated model was further validated using ERRAT, VERIFY 3D, and Ramachandran Plot embedded in SAVES v 6.0 server (Table S1).<sup>31,32</sup> For ERRAT evaluation, the overall quality factors of all the models showed good high resolution, and their value are greater than 93%. Specifically, I-TASSER server model scored the highest, with an overall quality factor of 96.1988, followed by Robetta server model with a score of 95.3216, AlphaFold model with a score of 93.4328 and Swiss-Model model with a score of 93.1343. VERIFY 3D was utilized to further calculate the percentage of amino acids that scored  $\geq 0.1$  in the 3D/1D profile. Among these models, only the model constructed by Robetta has an amino acid ratio equal to 80%, which meets the requirements, while the other three models are all below 80%. At last, we evaluate the protein models by Ramachandran plot. In Ramachandran Plot evaluation, the quality of Robetta model is as good as that of AlphaFold and Swiss-Model model. For the Robetta model, 93.3% of the residues were in the most favoured region and 5.4% in the allowed regions. These overall values indicated that the Robetta structure employed the best quality in the range of the theoretical protein structure models (Figure 1C). Therefore, the protein model constructed by Robetta server was used for the docking study. Then, GIT1/ $\beta$ -Pix were obtained to GIT1 protein model by referring to the crystal structure of GIT2/ $\beta$ -Pix complex from *Mus musculus* (PDB ID: 6JMT). The aligned complex was prepared by the protein prepare module of Sybyl-X 2.0 software and the optimized structure of the complex was chosen for the following MD study.

### Molecular Dynamics Study to Explore the Binding Pocket of GIT1

To determine the key residues of the binding pocket of GIT1, we conducted a 40 ns molecular dynamic simulation and the RMSD was used to explore the stability of the GIT1/ $\beta$ -Pix system (Figure 2A). From RMSD analysis, GIT1 attained its equilibrium (plateau) state at 5 ns, with the RMSD value of 2.28 Å (Figure 2B), while the  $\beta$ -Pix peptide reach stability

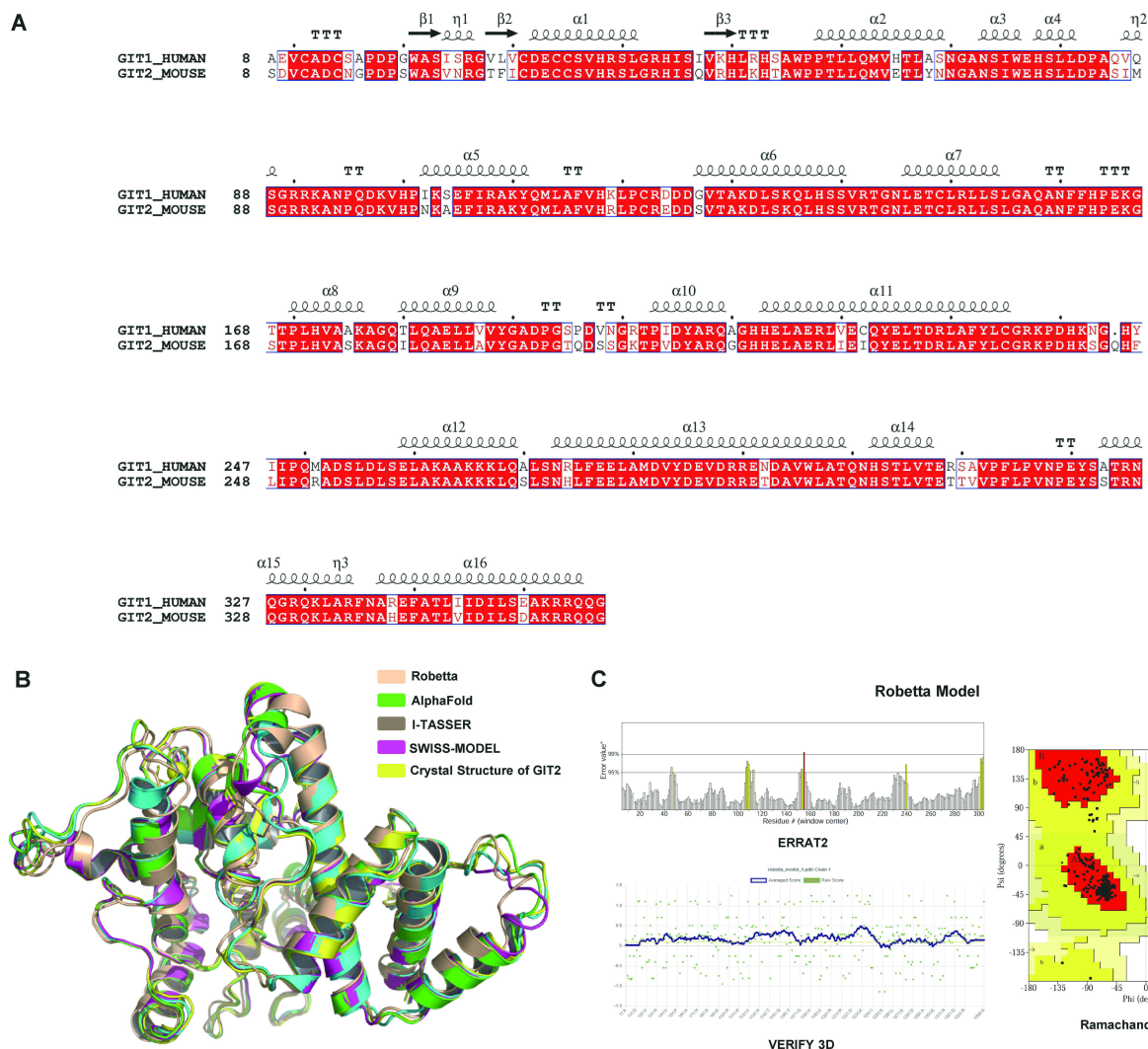


**Figure 1** The molecular modeling of GIT1/ $\beta$ -Pix. **(A)** The amino acid sequences alignment of the GIT1 and GIT2 using Clustal W. Highly conserved residues (conservation score > 0.7) were framed in blue according to physicochemical properties. The secondary structure depiction was based on the crystal structure of GIT2 from *Mus musculus* (PDB ID: 6JMT). **(B)** Robetta, AlphaFold, I-TASSER, Swiss-Model-predicted GIT1 3D cartoon structure and GIT2 crystal structure comparison (flesh, green, brown, purple, yellow, respectively). **(C)** The ERRAT, VERIFY 3D, and Ramachandran Plot graphs used to validate the chosen model (Robetta).

at 1 ns with RMSD of 0.52 Å (Figure 2B). Because of the multiple binding region between the  $\beta$ -Pix peptide and four helices of GIT1, the binding pose of the  $\beta$ -Pix has slight excursion. Compared with the docking structure, the H1 helix of GIT1 (from 260 to 271, near the binding interface) and adjacent loop (from 251 to 260, far from the binding interface) showed an obvious fluctuation, while other regions showed a rather slight shift (Figure 2A).

To further decipher the momentous residues for the binding pocket, the MM/GBSA free energy calculation was carried out. The binding free energy of GIT1/ $\beta$ -Pix system was  $-59.18 \pm 4.80$  kcal/mol, resulting from Van der Waals (VDW) energy ( $\Delta E_{vdw}$ ), electrostatic interaction energy ( $\Delta E_{ele}$ ), electrostatic contribution solvation free energy ( $\Delta G_{GB}$ ), and nonpolar solvation free energy ( $\Delta G_{SA}$ ) (Table 1). Obviously,  $\Delta E_{ele}$  terms made the greatest contribution to the assembly, indicating that VDW interactions generated the primary binding energy in the system.

To analyze the specific interactions in the system, the hydrogen bond analyses were carried out based on the MD simulation. During the MD simulation, the hydrogen bonds between SER322 (GIT1) and ASP532 ( $\beta$ -Pix), ASP346 (GIT1) and TYR542 ( $\beta$ -Pix), as well as ARG274 (GIT1) and GLU531 ( $\beta$ -Pix) were found in more than 10% of the frames of the MD trajectory (Table S2). Besides, the decomposition energy GIT1/ $\beta$ -Pix system (Figure 2C) suggested that ALA264, LEU268, LEU271, ARG274, LEU275, LEU279, SER322, ARG325, LEU343, and ASP346 of GIT1

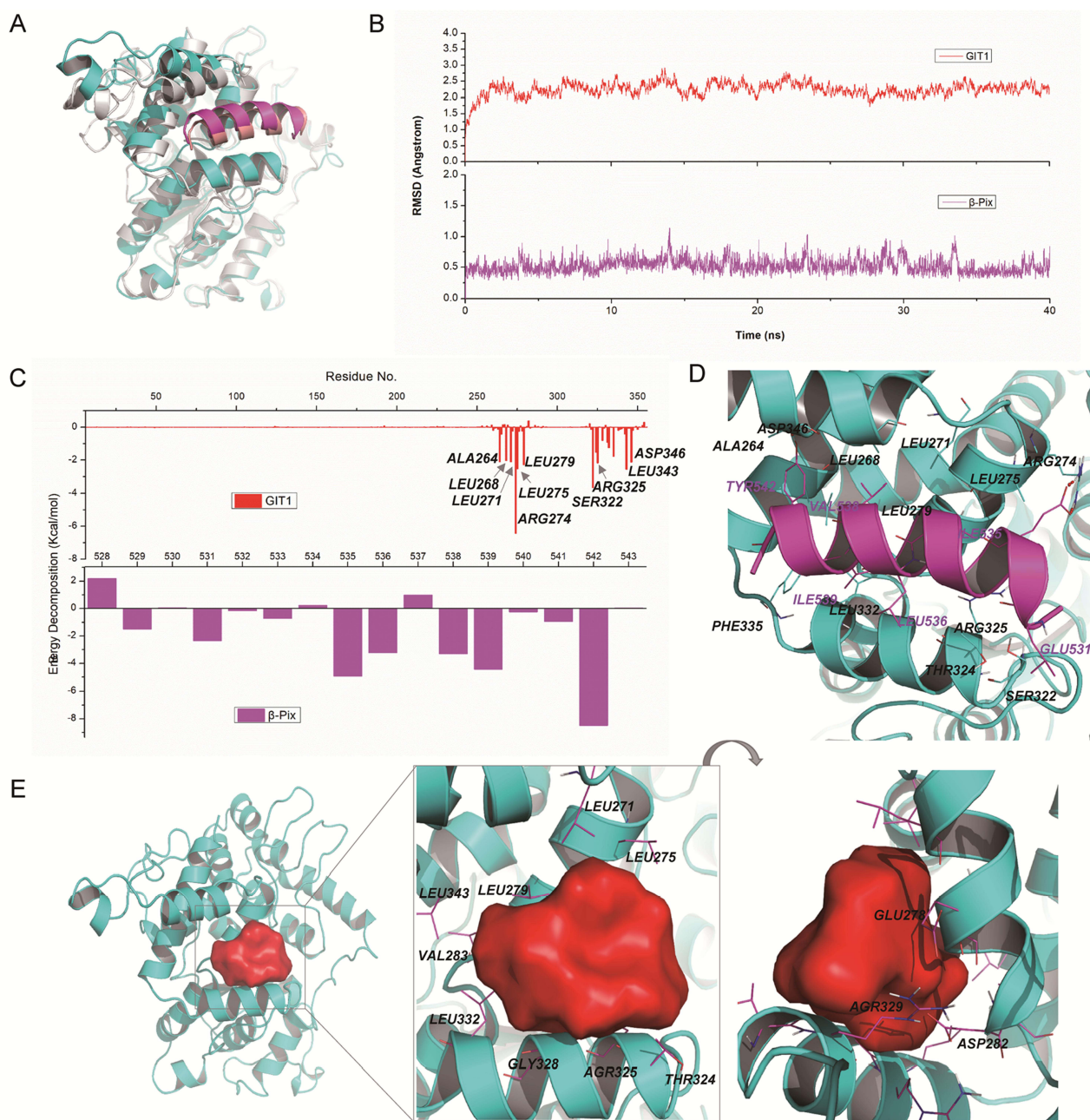


**Figure 2** Molecular dynamics study to explore the binding pocket of GIT1. **(A)** The AI model superimposed on the last configuration after 40 ns of simulation for GIT1 and  $\beta$ -Pix peptide. The initial and the last configurations of GIT1 were shown in grays and cyans, respectively, while the initial and the last configurations of  $\beta$ -Pix were shown in salmon and magenta, respectively. **(B)** The root mean square deviation (RMSD) of GIT1 and  $\beta$ -Pix peptide. **(C)** Binding free energy decomposition of GIT1 and  $\beta$ -Pix peptide system. **(D)** The key residues for the binding interaction of GIT1 and  $\beta$ -Pix peptide. **(E)** The binding pocket of GIT1.

contributed favourable energies lower than  $-2.0$  kcal/mol. Among these residues, there are hydrogen bonds between SER322 (GIT1) and ASP532 ( $\beta$ -Pix), ASP346 (GIT1) and TYR542 ( $\beta$ -Pix), as well ARG274 (GIT1) and GLU531 ( $\beta$ -Pix), whereas the binding interaction between ALA264, LEU268, LEU271, LEU275, LEU279, SER322, and LEU343

**Table I** Components of the Binding Free Energy (Kcal/Mol) of GIT1/ $\beta$ -Pix System Calculated by MM/GBSA Approach

$\Delta E_{vdw}$	$\Delta E_{ele}$	$\Delta G_{GB}$	$\Delta G_{SA}$	$\Delta Total$
$-71.8 \pm 4.6$	$-485.1 \pm 27.7$	$508.6 \pm 26.0$	$-11.0 \pm 0.6$	$-59.2 \pm 4.8$

with  $\beta$ -Pix peptide was hydrophobic interaction from the side chain of GIT1 and  $\beta$ -Pix (Figure 2D). Other residues, including PHE335 (GIT1), THR324 (GIT1), and Leu332 (GIT1) also proved important to the interaction of hydrophobic interaction with energy contributions lower than  $-1.0$  kcal/mol. Based on these results, we established the binding pocket by Sybyl-X 2.0 program (Figure 2E), which is formed by LEU271, LEU275, GLU278, LEU279, ASP282, LEU283, THR324, AGR325, GLY328, AGR329, LEU332 and LEU343.

## Virtual Screening and Identification of Potential GIT1 Inhibitors

Using the established docking model,<sup>15</sup> we performed high-throughput docking toward commercial library *ChemBridge* containing over 1.3 million compounds in Sybyl-X 2.0 program (Figure 3). Fifty compounds with highest total scores were chosen from two rounds of docking and further analyzed for their scaffold types and other docking parameters (detailed information shows in Table S3). Finally, nine small-molecule compounds were chosen for the following research after comprehensive consideration. Information of the nine compounds outperformed in the virtual screening were shown in Figure 3.

In order to determine whether these compounds directly bind to GIT1, the kinetic parameters of the binding affinity of the nine candidate compounds to GIT1 were detected using a biolayer interferometry (BLI) assay. The results showed that 17302836 has highest affinity to GIT1 among these compounds with a  $K_D$  value of  $84.1 \pm 2.0$   $\mu$ M (Figure 4). Compounds 63329390 and 82892519 were less affinitive ( $K_D$  values were  $150.4 \pm 3.5$  and  $188.3 \pm 4.2$   $\mu$ M, respectively,

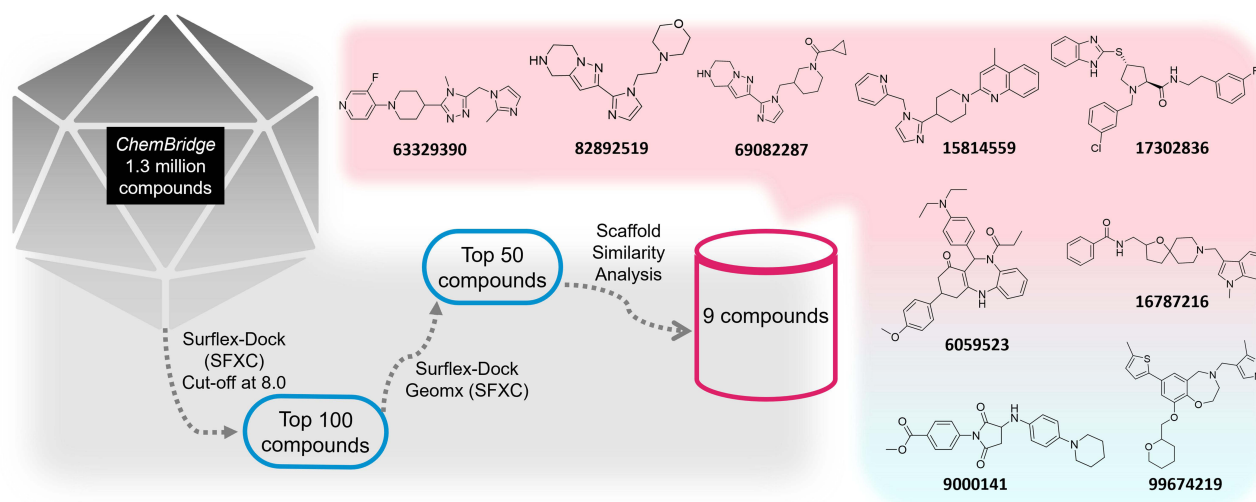


**Figure 3** The workflow of the compound screening process.

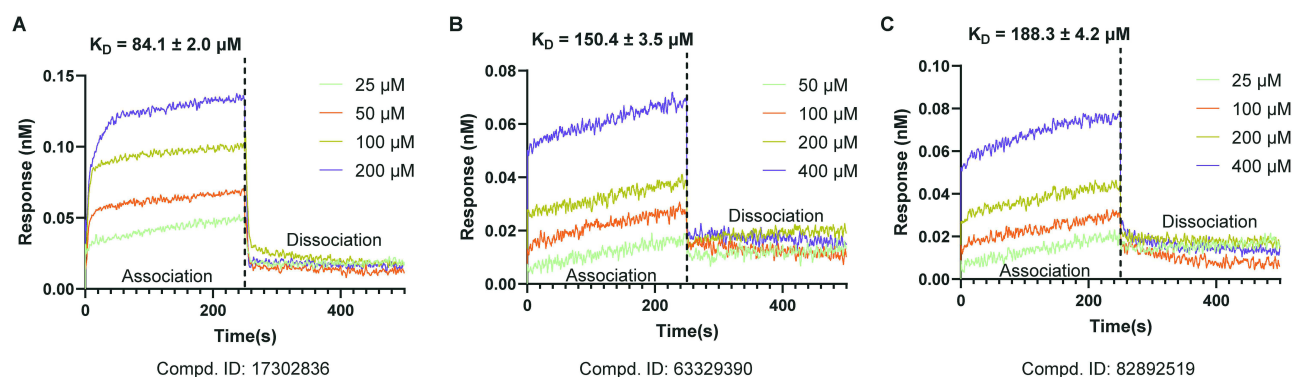


**Figure 4** Kinetic measurement of the binding affinity of the compounds 17302836 (A), 63329390 (B) and 82892519 (C) to GIT1 by BLI assay. Concentrations ranging from 25 to 400  $\mu$ M with real-time response for each step of the kinetic assay were shown.

**Table 2** The  $K_D$  Values of 9 Small-Molecule Compounds by BLI

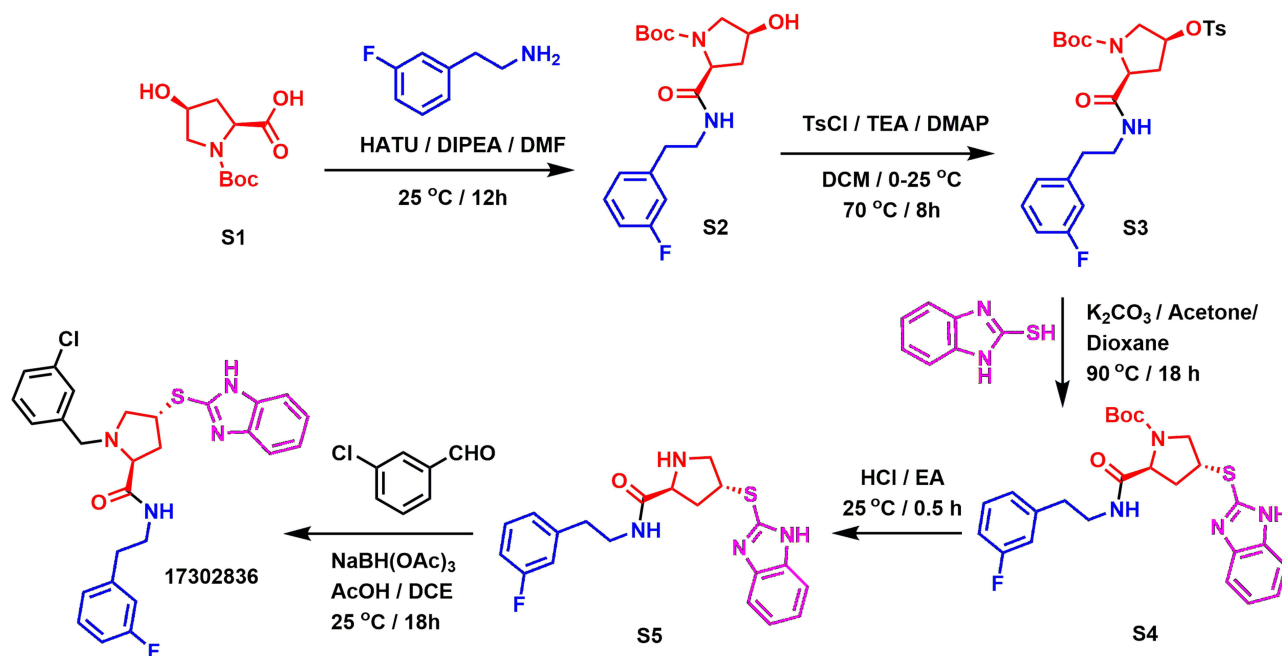
ZINC No.	Score	$K_D$ value <sup>a</sup>
63329390	9.7101	150.4±3.5
69082287	9.6553	614.5±198.5
16787216	9.393	1257.0±136.1
15814559	8.8705	6925.0±3266.0
6059523	8.8411	555.3±50.0
17302836	8.6503	84.1±2.0
82892519	8.4926	188.3±4.2
99674219	8.3766	2629.0±26.6
9000141	8.3252	578.7±21.5

**Notes:** <sup>a</sup>Each value represents the mean ± standard deviation of three experiments.

Figure 4), while others showed only slight affinity ( $K_D$  values over 500  $\mu$ M). The detailed  $K_D$  values of all other compounds were shown in Table 2.

## Synthesis of 17302836

To obtain large amount of 17302836 for further research, we established a de novo synthesis strategy (Scheme 1), starting from a proline derivative S1 and a phenethylamine substrate. The amide product S2 was generated smoothly, after which the hydroxy group was protected to provide S3 for the next substitution. The thiobenzimidazole moiety was then conjugated to the molecule via a SN2 reaction. S5 was then obtained after deprotection of Boc and subsequent assembly of the substituted benzyl to the *N* atom provided the target product. Generally, compound 17302836 could be obtained in five steps with acceptable yield, starting from simple substrates and concise reactions (see Supplementary Methods for details and Figure S3 for the spectrum).



**Scheme 1** The synthetic route of 17302836. DCM for dichloromethane, EtOAc for ethylacetate, DIPEA for *N,N*-diisopropylethylamine, DMF for *N,N*-dimethylformamide, HATU for 1-[bis(dimethylamino)methylene]-1*H*-1,2,3-triazolo[4,5-*b*]pyridinium 3-oxid hexafluoro-phosphate, TEA for Triethylamine, DMAP for 4-dimethylaminopyridine.

## Inhibition of 17302836 Against Invasion and Metastasis in Gastrointestinal Neoplasms

After determining the direct interaction between 17302836 and GIT1, we next investigated whether compound 17302836 could effectively inhibit tumor invasion and metastasis via interfering the GIT1/ $\beta$ -Pix interaction. Based on our previous study,<sup>15</sup> we chose gastrointestinal tumor cell lines including stomach cancer cell MGC803 and colorectal cancer cell HCT116 as representatives. First, the cell viability was detected using CCK8 assay to evaluate the toxicity of 17302836 in cell lines MGC803 and HCT116. The result showed that the compound did exhibit cytotoxicity in both cells under high concentrations, with  $IC_{50}$  values  $33.56 \pm 7.45 \mu\text{M}$  and  $15.17 \pm 0.88 \mu\text{M}$ , respectively (Figure S1). Then in the transwell assay to evaluate the anti-invasive effect of the compound, concentrations within “safe” concentration range were selected for to exclude the cytotoxicity-induced cell loss that could influence the anti-invasive activity evaluation. Under comparatively low concentrations, compound 17302836 could still exhibit considerable anti-invasive activity. Concentrations 1.0, 5.0 and 10  $\mu\text{M}$  were tested for HCT116, while 2.0, 8.0 and 16.0  $\mu\text{M}$  for MGC803 (Figure 5A). Obvious inhibition could be observed under 5.0  $\mu\text{M}$  concentration for HCT116, which was more sensitive to 17302836 treatment. MGC803 was less sensitive, but 8.0  $\mu\text{M}$  17302836 was still enough to induce obvious inhibition on cell invasion.

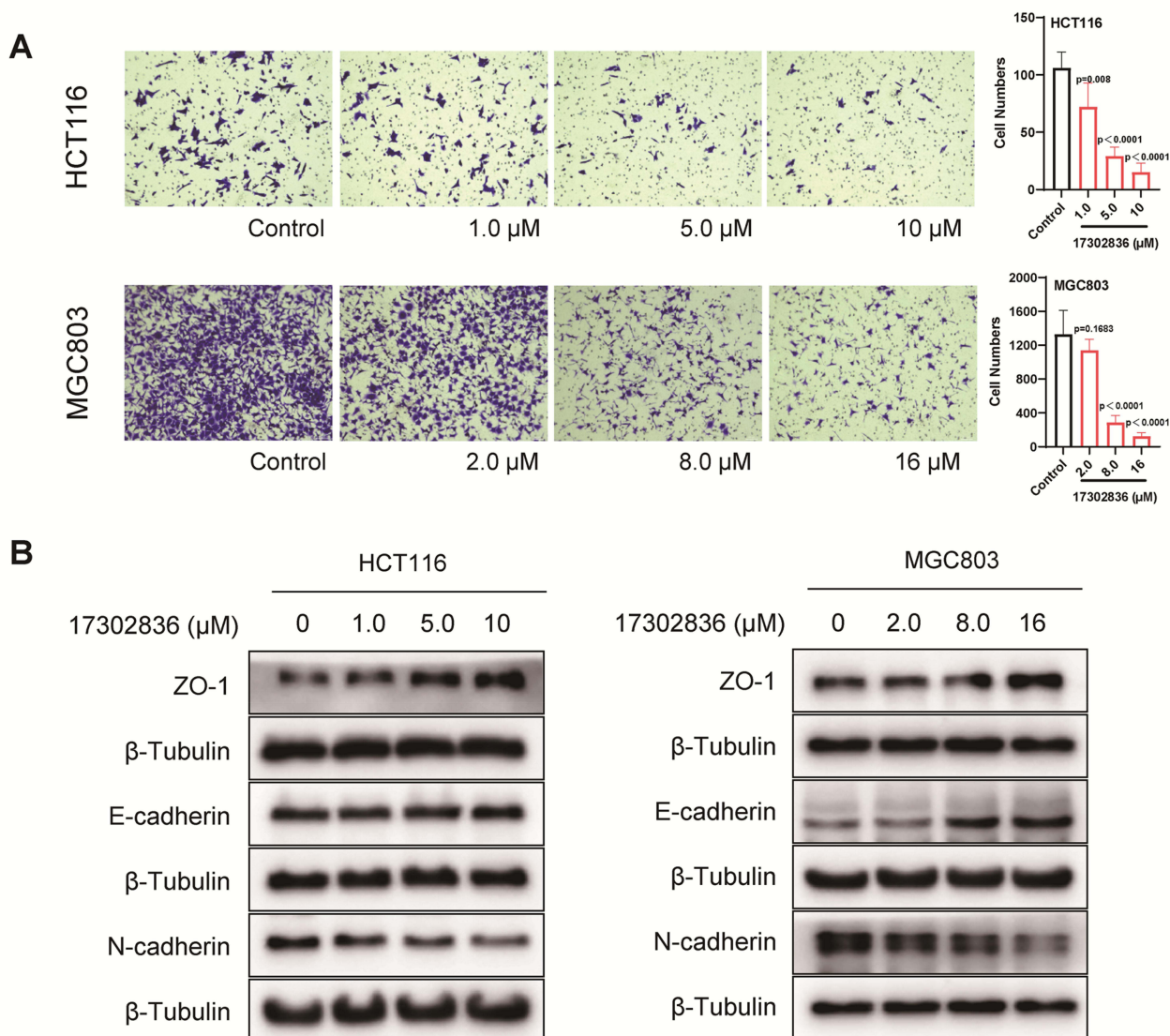


**Figure 5** 17302836 suppresses invasion in gastrointestinal cancer cell lines HCT116 and MGC803. **(A)** Anti-invasion effect of 17302836 in HCT116 and MGC803 detected by transwell (n=6); **(B)** EMT-related protein expression to detect tumor invasion and metastasis in HCT116 and MGC803 detected by Western blotting (n=5).

Moreover, EMT-related protein expression was detected to study the underlying mechanism of the anti-invasive effect of 17302836 in MGC803 and HCT116. The upregulation of effector molecules ZO-1 and E-cadherin, as well as the downregulation of N-cadherin revealed that 17302836 inhibited the EMT progression to affect the cell invasion (Figure 5B and Figure S2). In conclusion, compound 17302836 effectively inhibit cell invasion in gastric and colorectal cell lines HCT116 and MGC803, and exhibited better activity than the reported inhibitor,<sup>15</sup> which is more promising to be developed as a lead compound targeting GIT1/ $\beta$ -Pix.

## Binding Mode Analysis of 17302836 to GIT1 Based on Molecular Dynamics (MD) Simulation

One hundred nanosecond MD simulation was performed to study the interaction and the conformational stability of 17302836 to the active site of GIT1 binding to  $\beta$ -pix. The stability of 17302836 binding to GIT1 protein was evaluated by the RMSD and RMSF analysis. As shown in Figure 6A, the RMSD trajectory of the GIT1 reached stability at  $\sim 30$  ns, with the RMSD value of  $3.4273 \pm 0.2909$  Å, while the ligand 17302836 had a large drift at the initial stage of simulation, and tended to be stable at 30 ns, with the RMSD value of  $2.5524 \pm 0.1448$  Å (Figure 6A). The per-residue RMSF analysis showed that the fluctuations of the residues decreased in binding site such as LEU288, ASP291, LYS276, while that in other regions were slightly increased (Figure 6B). In addition, a total of 100 frames extracted from equilibration trajectory were utilized to the MM/GBSA free energy calculation. The result showed that 17302836 could strongly bind to GIT1 with total binding free energy ( $\Delta G$ ) of  $-53.3762$  kcal/mol. The detailed van der Waals interaction energy ( $\Delta E_{vdw}$ ), electrostatic interaction energy ( $\Delta E_{ele}$ ), electrostatic salvation energy (polar contribution) ( $\Delta G_{GB}$ ) and nonelectrostatic salvation component (nonpolar contribution) ( $\Delta G_{SA}$ ) are listed in Table 3.

To accurately investigate the binding interaction, the energy decomposition strategy was employed for identification of key amino acid residues. First, the aromatic rings (phenyl, benzimidazole and pyrrole) of 17302836 were surrounded by the hydrophobic chamber site and mainly formed hydrophobic interactions with 6 residues (LEU288, GLU287, ALA273, LYS275, LEU341, LEU352). Among them, LEU288 donated the largest energy contribution with the value of  $-4.1997$  kcal/mol, mainly contributed by van der Waals for hydrophobic interactions (Figure 6C). Second, the nitrogen

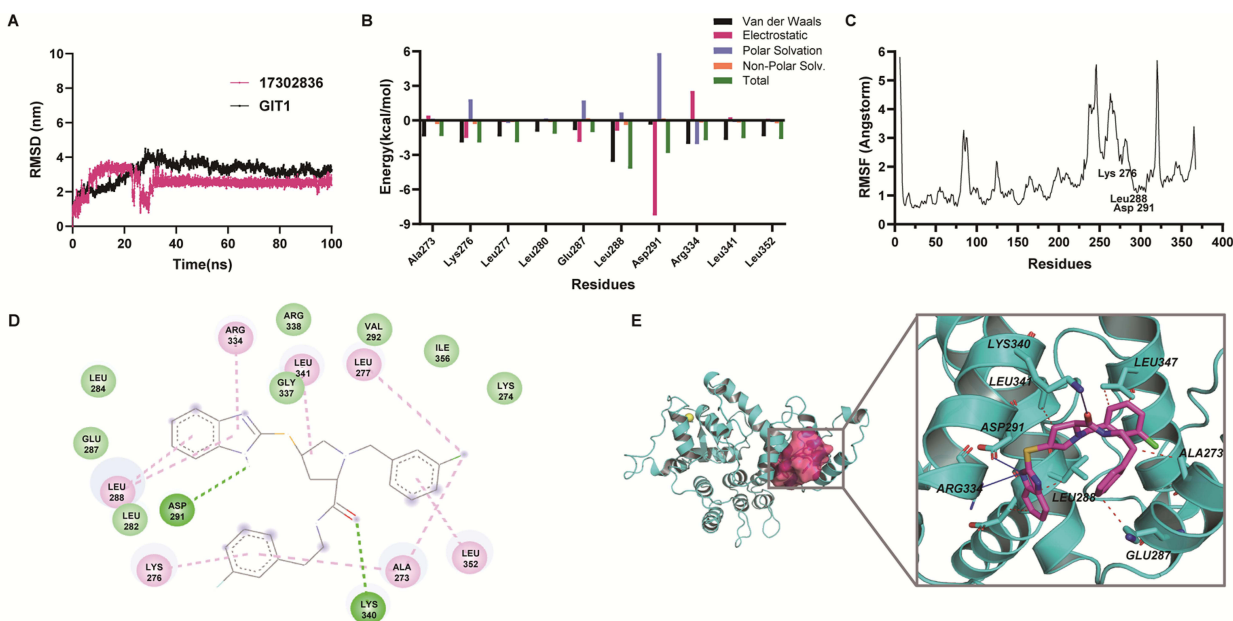


**Figure 6** Molecular dynamics simulation analysis between GIT1 and 17302836. (A) and (B) Time evolution plot of root mean square deviation (RMSD) of GIT1 (black) – 17302836 complex (red) and root mean square fluctuation (RMSF) of GIT1; (C) Free energy contributions of key amino acid residues calculated by MM/GBSA method; (D) The 2D representation of the MD result of the compound (17302836) binds with GIT1; (E) Key residues for the interactions in GIT1/17302836 systems during the MD simulations. The binding pockets of GIT1 was shown as surface and colored by magentas (left). The key residues of GIT1 were displayed in sticks and the hydrogen bonds are shown with blue lines, while the hydrophobic interactions were shown as red dashed lines. The compound 17302836 is colored magenta and shown by sticks (right).

**Table 3** Components of the Binding Free Energy (Kcal/Mol) of 17302836 Docking with GIT1 Calculated by MM/GBSA Approach

$\Delta E_{vdw}$	$\Delta E_{ele}$	$\Delta G_{GB}$	$\Delta G_{SA}$	$\Delta Total$
-48.1±2.7	-26.5±7.2	27.1±6.0	-5.9±0.3	-53.4±3.1

of benzimidazole also possessed a hydrogen bond interaction with ASP291 with a distance value of 2.74 Å. The nitrogen atom also formed a hydrogen binding with ARG334 with 3.64 Å (Figure 6C). These results show that these amino acids played an important role in the combination of 17302836 and GIT1. The detailed interaction between GIT1 and compound 17302836 was shown in Figure 6D and E.

## Discussion

Gastrointestinal cancers including gastric cancer and colorectal cancer are highly malignant cancer types, and are the third and fifth leading cause of cancer deaths in China, respectively.<sup>1</sup> The high occurrence of cancer metastasis is the main cause of tumor progression and mortality. To discover new targets and therapeutic agents for intervening metastasis has been long focused and deemed as promising strategies for cancer treatment. Studies have shown that GIT1/ $\beta$ -Pix complex plays a vital role in tumor invasion and metastasis.<sup>15,22,33</sup> An endogenous protein Naa10p can interrupt GIT1/ $\beta$ -Pix interaction and thus interfere the invasion and metastasis in lung cancer.<sup>18</sup> This effect was also verified in gastric cancer by our group using a small-molecule compound.<sup>15</sup> Therefore, the inhibition of GIT1/ $\beta$ -Pix interaction is a potential strategy for prevention of tumor invasion and metastasis. As small-molecule compounds are more suitable for drug development,<sup>34</sup> we have focused on the development of small-molecule GIT1/ $\beta$ -Pix inhibitors with high selectivity, high affinity and low toxicity. However, it is well-recognized that to find the inhibitors for PPI targets such as GIT1/ $\beta$ -Pix is a challenging task. In our previous work, 14-5-18 was identified from a self-constructed compound library with high degree of structural specificity, but no candidate was generated by conventional commercial library *ChemDiv*. As far as we know, 14-5-18 is still the only small-molecule inhibitor of GIT1/ $\beta$ -Pix. However, although the affinity 14-5-18 is fair ( $K_D = 7.7 \pm 0.1 \mu M$ ), its effective concentration for invasion and metastasis inhibition in vitro and in vivo is still high (concentrations 10–50  $\mu M$  were used in cell assays). Moreover, its scaffold, which contains continuous bridged and spiro rings, is too complex for further development.<sup>15</sup> Thus, more small-molecule inhibitors with simpler scaffold, high efficiency and low toxicity are in great demand. In this study, we identified a novel small-molecule inhibitor 17302836 targeting the GIT1/ $\beta$ -Pix complex in the *ChemBridge* library by virtual screening and direct binding detection by BLI assay. Further experiments also confirmed that 17302836 exhibited good inhibition of cell invasion in HCT116 and MGC803 cell lines with only slight cytotoxicity. It is interesting that 17302836 outperformed in efficient concentrations (1.0–10  $\mu M$  for HCT116 and 2.0–16  $\mu M$  for MGC803) compared with 14-5-18, although its affinity was lower ( $K_D$  to GIT1 is  $84.1 \pm 2.0 \mu M$ ). The underlying mechanism might be the better cell penetration or solubility of 17302836. Furthermore, the flexible structure of 17302836 could be easier for structural modification, comparing with the rigid scaffold of 14-5-18. The abovementioned advantages suggest that 17302836 could be more promising for further development as drug candidate (Figure 7).

In our previous work, the fluorescence polarization (FP) assay was used to detect the potential inhibitory activity of the hit compounds, which resulted in very limited compounds for further development when we cut off at  $IC_{50} > 100 \mu M$ .<sup>15</sup> In the present work, BLI was used to determine the direct binding. As the  $K_D$  value could be generated in a single experiment, more compounds were possible to be selected for further evaluation. And 17302836 have shown good potency even if its affinity was not quite satisfying. Therefore, expect for the difference between compound libraries, we demonstrated that using BLI to evaluate the direct binding would be a more suitable evaluation assay.

At the same time, the major limitation of this study is lack of animal experiments to evaluate the pharmacological and pharmacokinetic properties of 17302836, as well as more solid evidence to exclude its possible off-target effects. These aspects are under investigation, and the results will be demonstrated in due course.

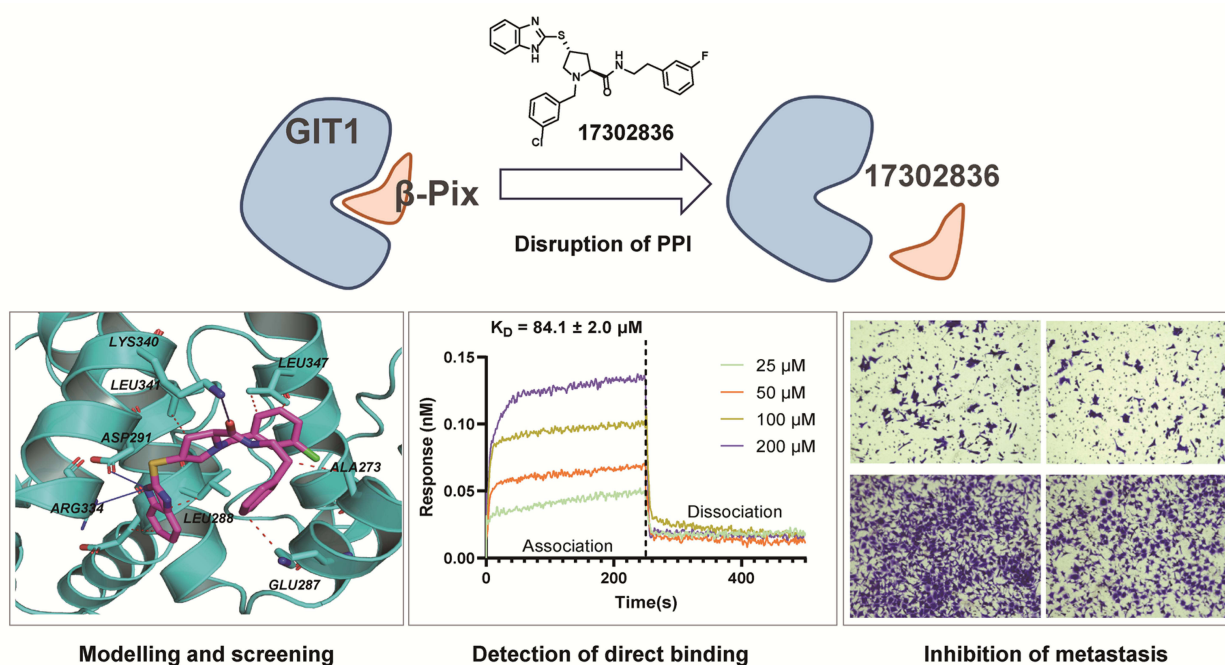


**Figure 7** The graphic abstract. 17302836, a compound obtained through virtual screening, validated by direct binding, could disrupt the GIT1/ $\beta$ -Pix protein-protein interaction and thus inhibit metastasis of gastrointestinal cancer cells.

## Conclusion

In conclusion, in this study, a small-molecule inhibitor 17302836 targeting GIT1/ $\beta$ -Pix interaction was successfully identified by virtual screening. In gastric cancer and colorectal cancer cells, 17302836 showed good in vitro anti-invasion activity. This study provides a promising candidate for developing new GIT1/ $\beta$ -Pix inhibitors for tumor treatment.

## Acknowledgments

We thank Professor Jinwei Zhu at Bio-X Institutes, Shanghai Jiao Tong University for providing the purified GIT1 protein used in this study. This research is funded by National Natural Science Foundation of China (82273775 and 22007100), Outstanding Youth Fund of Chongqing (2023NSCQ-JQX0081), Natural Science Foundation of Chongqing (CSTB2022NSCQ-MSX0069), National Key Research and Development Program of China (2022YFC2502501), the Senior Medical Talents Program of Chongqing for Young and Middle-aged people and Kuanren Talents Program of The Second Affiliated Hospital of Chongqing Medical University.

## Disclosure

The authors report no competing interests in this work.

## References

1. Siegel RL, Miller KD, Wagle NS, et al. Cancer statistics, 2023. *CA Cancer J Clin*. 2023;73(1):17–48. doi:10.3322/caac.21763
2. Fares J, Fares MY, Khachfe HH, et al. Molecular principles of metastasis: a hallmark of cancer revisited. *Signal Transduct Target Ther*. 2020;5(1):28. doi:10.1038/s41392-020-0134-x
3. Cooke M, Baker MJ, Kazanietz MG. Rac-GEF/Rac Signaling and Metastatic Dissemination in Lung Cancer. *Front Cell Dev Biol*. 2020;8:118. doi:10.3389/fcell.2020.00118
4. Liu Y, Lacal J, Firtel RA, et al. Connecting G protein signaling to chemoattractant-mediated cell polarity and cytoskeletal reorganization. *Small GTPases*. 2018;9(4):360–364. doi:10.1080/21541248.2016.1235390
5. Yoo SM, Antonyak MA, Cerione RA. The adaptor protein and Arf GTPase-activating protein Cat-1/Git-1 is required for cellular transformation. *J Biol Chem*. 2012;287(37):31462–31470. doi:10.1074/jbc.M112.353615
6. Frank SR, Hansen SH. The PIX-GIT complex: a G protein signaling cassette in control of cell shape. *Semin Cell Dev Biol*. 2008;19(3):234–244. doi:10.1016/j.semcdb.2008.01.002

7. Zhou W, Li X, Premont RT. Expanding functions of GIT Arf GTPase-activating proteins, PIX Rho guanine nucleotide exchange factors and GIT-PIX complexes. *J Cell Sci.* 2016;129:1963–1974. doi:10.1242/jcs.179465
8. Li L, Tang P, Zhou Z, et al. GIT1 regulates angiogenic factor secretion in bone marrow mesenchymal stem cells via NF- $\kappa$ B/Notch signalling to promote angiogenesis. *Cell Prolif.* 2019;52:e12689.
9. Xu T, Gao P, Huang Y, et al. Git1-PGK1 interaction achieves self-protection against spinal cord ischemia-reperfusion injury by modulating Keap1/Nrf2 signaling. *Redox Biol.* 2023;62:102682.
10. Huang YF, Gu CJ, Wang Q, et al. The protective effort of GPCR kinase 2-interacting protein-1 in neurons via promoting Beclin1-Parkin induced mitophagy at the early stage of spinal cord ischemia-reperfusion injury. *FASEB J.* 2020;34:2055–2074. doi:10.1096/fj.201902047R
11. Kim MJ, Biag J, Fass DM, et al. Functional analysis of rare variants found in schizophrenia implicates a critical role for GIT1-PAK3 signaling in neuroplasticity. *Mol Psychiatry.* 2017;22:417–429. doi:10.1038/mp.2016.98
12. Fass DM, Lewis MC, Ahmad R, et al. Brain-specific deletion of GIT1 impairs cognition and alters phosphorylation of synaptic protein networks implicated in schizophrenia susceptibility. *Mol Psychiatry.* 2022;27(8):3272–3285. doi:10.1038/s41380-022-01557-z
13. Chen J, Yang P, Yang J, et al. GIT1 is a novel prognostic biomarker and facilitates tumor progression via activating ERK/MMP9 signaling in hepatocellular carcinoma. *Oncotargets Ther.* 2015;8:3731–3742. doi:10.2147/OTT.S96715
14. Chang JS, Su CY, Yu WH, et al. GIT1 promotes lung cancer cell metastasis through modulating Rac1/Cdc42 activity and is associated with poor prognosis. *Oncotarget.* 2015;6(34):36278–36291. doi:10.18632/oncotarget.5531
15. Gu J, Peng RK, Guo CL, et al. Construction of a synthetic methodology-based library and its application in identifying a GIT/Pix protein-protein interaction inhibitor. *Nat Commun.* 2022;13(1):7176. doi:10.1038/s41467-022-34598-7
16. Zhang J, Zhang J, Liu W, et al. UBTf facilitates melanoma progression via modulating MEK1/2-ERK1/2 signalling pathways by promoting GIT1 transcription. *Cancer Cell Int.* 2021;21(1):543. doi:10.1186/s12935-021-02237-8
17. Zhang Z, Hu P, Xiong J, et al. Inhibiting GIT1 reduces the growth, invasion, and angiogenesis of osteosarcoma. *Cancer Manag Res.* 2018;10:6445–6455. doi:10.2147/CMAR.S181066
18. Hua KT, Tan CT, Johansson G, et al. N- $\alpha$ -acetyltransferase 10 protein suppresses cancer cell metastasis by binding Pix proteins and inhibiting Cdc42/Rac1 activity. *Cancer Cell.* 2011;19(2):218–231. doi:10.1016/j.ccr.2010.11.010
19. Zhu J, Zhou Q, Xia Y, et al. GIT/Pix Condensates Are Modular and Ideal for Distinct Compartmentalized Cell Signaling. *Mol Cell.* 2020;79(5):782–796.e6. doi:10.1016/j.molcel.2020.07.004
20. Batool M, Ahmad B, Choi S. A Structure-Based Drug Discovery Paradigm. *Int J Mol Sci.* 2019;20(11):2783. doi:10.3390/ijms20112783
21. Yan Y, Tao H, He J, et al. The HDock server for integrated protein-protein docking. *Nat Protoc.* 2020;15(5):1829–1852. doi:10.1038/s41596-020-0312-x
22. Forli S, Huey R, Pique ME, et al. Computational protein-ligand docking and virtual drug screening with the AutoDock suite. *Nat Protoc.* 2016;11(5):905–919. doi:10.1038/nprot.2016.051
23. Luo Y, Yu S, Tong L, et al. Synthesis and biological evaluation of new homocamptothecin analogs. *Eur J Med Chem.* 2012;54:281–286. doi:10.1016/j.ejmech.2012.05.002
24. Bhadra P, Siu SWI. Refined Empirical Force Field to Model Protein-Self-Assembled Monolayer Interactions Based on AMBER14 and GAFF. *Langmuir.* 2019;35(29):9622–9633. doi:10.1021/acs.langmuir.9b01367
25. Maier JA, Martinez C, Kasavajhala K, et al. ff14SB: improving the Accuracy of Protein Side Chain and Backbone Parameters from ff99SB. *J Chem Theory Comput.* 2015;11:3696–3713. doi:10.1021/acs.jctc.5b00255
26. Suresh PK, Divya N, Nidhi S, et al. Phenylethanol-Bovine Serum Albumin interactions - modeling plasma protein - drug binding: a multi-spectroscopy and in silico-based correlation. *Spectrochim. Acta A Mol, Biomol, Spectrosc.* 2018;193:523–527. doi:10.1016/j.saa.2017.12.069
27. Laskowski RA, Swindells MB. LigPlot+: multiple ligand-protein interaction diagrams for drug discovery. *J Chem Inf Model.* 2011;51(10):2778–2786. doi:10.1021/ci200227u
28. Çınaroğlu SS, Timuçin E. Comprehensive evaluation of the MM-GBSA method on bromodomain-inhibitor sets. *Brief Bioinform.* 2020;21(6):2112–2125. doi:10.1093/bib/bbz143
29. Madeira F, Pearce M, Tivey ARN, et al. Search and sequence analysis tools services from EMBL-EBI in 2022. *Nucleic Acids Res.* 2022;50:W276–W279.
30. Robert X, Gouet P. Deciphering key features in protein structures with the new ENDscript server. *Nucleic Acids Res.* 2014;42(W1):W320–W324. doi:10.1093/nar/gku316
31. Laskowski RA, MacArthur MW, Moss DS, Thornton JM. PROCHECK: a Program to Check the Stereochemical Quality of Protein Structures. *J Appl Crystallogr.* 1993;26(2):283–291. doi:10.1107/S0021889892009944
32. Hooft RWW, Vriend G, Sander C, et al. Errors in Protein Structures. *Nature.* 2020;381(6580):272. doi:10.1038/381272a0
33. Chien MH, et al. N- $\alpha$ -acetyltransferase 10 protein promotes metastasis by stabilizing matrix metalloproteinase-2 protein in human osteosarcomas. *Cancer Lett.* 2018;433:86–98. doi:10.1016/j.canlet.2018.06.033
34. Prueksaritanont T, Tang C. ADME of biologics—what have we learned from small molecules? *AAPS J.* 2012;14(3):410–419. doi:10.1208/s12248-012-9353-6

## Drug Design, Development and Therapy

Dovepress

### Publish your work in this journal

Drug Design, Development and Therapy is an international, peer-reviewed open-access journal that spans the spectrum of drug design and development through to clinical applications. Clinical outcomes, patient safety, and programs for the development and effective, safe, and sustained use of medicines are a feature of the journal, which has also been accepted for indexing on PubMed Central. The manuscript management system is completely online and includes a very quick and fair peer-review system, which is all easy to use. Visit <http://www.dovepress.com/testimonials.php> to read real quotes from published authors.

Submit your manuscript here: <https://www.dovepress.com/drug-design-development-and-therapy-journal>